A Journal of the Gesellschaft Deutscher Chemiker

Angewandte International Edition GDCh Chemie

www.angewandte.org

Accepted Article

Title: Aptamer-PROTAC Conjugates (APCs) for Tumor-specific Targeting in Breast Cancer

Authors: Shipeng He, Fei Gao, Junhui Ma, Haoqian Ma, Guoqiang Dong, and Chunquan Sheng

To be cited as: *Angew. Chem. Int. Ed.* 10.1002/anie.202107347

Link to VoR: https://doi.org/10.1002/anie.202107347

WILEY-VCH

10.1002/anie.202107347

RESEARCH ARTICLE

WILEY-VCH

Aptamer-PROTAC Conjugates (APCs) for Tumor-specific Targeting in Breast Cancer

Shipeng He,†[b] Fei Gao,†[b] Junhui Ma,†[a] Haoqian Ma,[a] Guoqiang Dong,*[a] Chunquan Sheng,*[a]

†These authors made equal contributions to this work.

[a] J. Ma, H. Ma, Prof. G. Dong,* Prof. C. Sheng*
School of Pharmacy, Second Military Medical University,
Shanghai 200433, China
E-mail: gdong@smmu.edu.cn, shengcq@smmu.edu.cn
[b] S. He, F. Gao
Institute of Translational Medicine, Shanghai University,
Shanghai 200444, China

Supporting information for this article is given via a link at the end of the document.

Abstract: Development of proteolysis targeting chimeras (PROTACs) is emerging as a promising strategy for targeted protein degradation. However, the drug development using the heterobifunctional PROTAC molecules is generally limited by poor membrane permeability, low in vivo efficacy and indiscriminate distribution. Herein an aptamer-PROTAC conjugation approach was developed as a novel strategy to improve the tumor-specific targeting ability and in vivo antitumor potency of conventional PROTACs. As proof of concept, the first aptamer-PROTAC conjugate (APC) was designed by conjugating a BET-targeting PROTAC to the nucleic acid aptamer AS1411 (**AS**) via a cleavable linker. Compared with the unmodified BET PROTAC, the designed molecule (**APR**) showed improved tumor targeting ability in a MCF-7 xenograft model, leading to enhanced in vivo BET degradation and antitumor potency and decreased toxicity. Thus, the APC strategy may pave the way for the design of tumor-specific targeting PROTACs and have broad applications in the development of PROTAC-based drugs.

Introduction

Proteolysis targeting chimeras (PROTACs) are bifunctional small molecules that simultaneously bind to the target protein and an E3 ubiquitin ligase.[1] Mediated by the PROTAC, the target protein can be recognized by the E3 ligase, tagged with ubiquitin and degraded by the ubiquitin-proteasome system.[2] As an efficient approach for targeted protein degradation, PROTACs exhibit significant advantages over traditional small molecule drugs in terms of their catalytic profiles, high selectivity, ability to overcome drug resistance, and efficient blockade of undruggable targets. Recently, PROTACs have emerged as a promising technology in drug discovery, and numerous PROTACs have been reported, among which two compounds (ARV-110 and ARV-471) are currently being evaluated in clinical trials.[3] Despite these advantages, conventional PROTACs generally a have high molecular weight and high hydrophobicity, and their physicochemical properties are largely beyond the "rule of five" (RO5).[4] Thus, the development of conventional PROTACs into drugs is generally limited by their poor cell membrane permeability, unfavorable pharmacokinetic (PK) profiles, and lack of tumor-specific targeting.[5] Therefore, developing novel strategies to improve the water solubility, membrane permeability and tumor-targeting ability of conventional PROTACs is urgently needed.[6]

Targeted antitumor therapy has the advantages of increasing the enrichment of drugs in tumor tissues and reducing side effects.[7] Recently, antibody-drug conjugate (ADC)-mediated delivery[8] and folate-caged delivery[9] of PROTACs have been reported. However, ADCs usually consist of more than 1000 amino acids,[10] and their high molecular weight might lead to disadvantages in cell uptake, plasma half-life, immunogenicity, manufacturing cost, stability and so on.[11] In addition, ADCs are usually nonuniform, and the binding sites and the number of binding drugs vary among different antibodies, leading to difficulties in controlling the administration dose and complex pharmacokinetics.[12] Folate-caged PROTACs have been shown to exhibit improved degradation selectivity between cancer cells and normal cells. However, their in vivo antitumor activity and toxicity have not been explored. Therefore, the development of new delivery strategies to improve the tumor issue specificity and antitumor potency and decrease the toxicity of conventional PROTACs is highly desirable.

Aptamers are single-stranded nucleic acids that exhibit complex three-dimensional structures, such as stems, rings, hairpins, and G4 polymers.[13] They bind to the target protein with high specificity and affinity through hydrogen bonding, van der Waals forces, base stacking forces, and electrostatic effects.[14] Aptamers are also called "chemical antibodies" and have significant advantages with respect to other targeting vectors.[15] Aptamers are suitable for large-scale preparation because they can be automatically synthesized via DNA solid phase synthesis. Moreover, their structure can be easily modified to facilitate the efficient and controllable formation of multiple drug structures and improve water solubility. Importantly, aptamers exhibit good tissue penetration and favorable in vivo safety profiles without obvious immunogenicity.[16] Recently, aptamers have been widely used in targeted therapy against human tumors.[15] The nucleic acid aptamer AS1411 (**AS**) is rich in guanine bases and specifically recognizes and binds to nucleolin,[17] which is highly expressed on tumor cell membranes and is widely used as a biomarker for targeted antitumor therapy.[18] **AS** itself has good inhibitory activity against nucleolin-overexpressing tumors and is currently being evaluated in a phase II clinical trial.[19] In addition, **AS** is widely used as a transport agent for tumor-targeted

delivery of small molecule drugs.[18b] Inspired by the promising profiles of aptamers in targeted cancer therapy, we envisioned that conjugation of an aptamer to a conventional PROTAC would improve the tumor-targeting characteristics as well as antitumor potency of the original PROTAC. Thus, herein, we developed a novel aptamer-PROTAC conjugation strategy to improve the tumor-specific targeting of conventional PROTACs. The first aptamer-PROTAC conjugate (APC) was rationally designed by modifying the bromodomain and extra-terminal (BET) PROTAC with the **AS** aptamer and a cleavable linker. The conjugate showed excellent specificity for and potent effects on BET degradation in nucleolin-overexpressing MCF-7 breast cancer cells. The advantages of the APC were further highlighted by its excellent in vivo tumor targeting ability, potent antitumor efficacy and reduced side effects on normal organs. Therefore, the APC strategy may offer a valuable tool to diminish the shortcomings of conventional PROTACs by improving their water solubility, tumor targeting ability, and antitumor efficacy.

Results and Discussion

Rational design of AS-PROTAC conjugates. BET family proteins (BRD2, BRD3, BRD4 and BRDT) act as key epigenetic regulators that selectively recognize and bind to acetylated histones, thus converting chromatin into a conformation suitable for transcriptional elongation via RNA polymerase II (Pol II).[20] These proteins are regarded as promising antitumor targets that are closely related to the regulation of gene transcription and mediate the transcription of associated genes.[20] To date, numerous PROTACs for BET degradation have been developed.[21] Due to the well-established data available for BET PROTACs, they are generally used as a standard platform for mechanistic studies and methodology development.[22] In particular, a BET-targeting PROTAC (herein denoted compound **4**, **PRO**; **Scheme 1**) has been generally applied as a template PROTAC molecule for developing new PROTAC delivery strategies.[8a, 23] Therefore, the potent BET (BRD4) degrader **PRO** and the nucleolin-dependent aptamer **AS** were selected for a proof-of-concept study of APCs (**Figure 1a**). A well-defined molecular structure of PROTACs must be maintained to allow the formation of ternary complexes with the target protein and an E3 ubiquitin enzyme.[22a] Therefore, the attachment site in the structure of **PRO** is particularly important in the design of APCs, which should undergo targeted delivery into tumor cells and then release the original **PRO** molecule by disassociation of the linker. Structural analysis of **PRO** indicated that the VHL ligand contains a free hydroxyl group, which provided a suitable attachment site for the introduction of the linker and **AS**. Notably, this hydroxyl group is essential for VHL binding,[3, 24] and attachment of a linker and aptamer at this site would block the degrading activity of **PRO**. Thus, an ester-disulfide linker was designed to ensure intracellular release of **PRO** (**Figure 1b**). First, the aptamer **AS** can be selectively recognized by nucleolin-overexpressing tumor cells. Then, the disulfide bond is broken by nucleophilic attack of abundant endogenous glutathione (GSH) in tumor cells.[25] Finally, the newly formed free mercapto group can attack the carbon anhydride ester bond to release the **PRO** molecule. To evaluate the distribution, stability and antitumor activity of the designed APC (compound **APR**), a series of control molecules were also designed (**Figure 1b**). A cytosine-rich oligonucleotide sequence (**CRO**), which represents a nonspecific DNA sequence, was selected as the control for **AS**. Fluorescein amidate (Fam) or cyanine3 (Cy3) modifications were designed to visualize the specific targeting of conjugates.

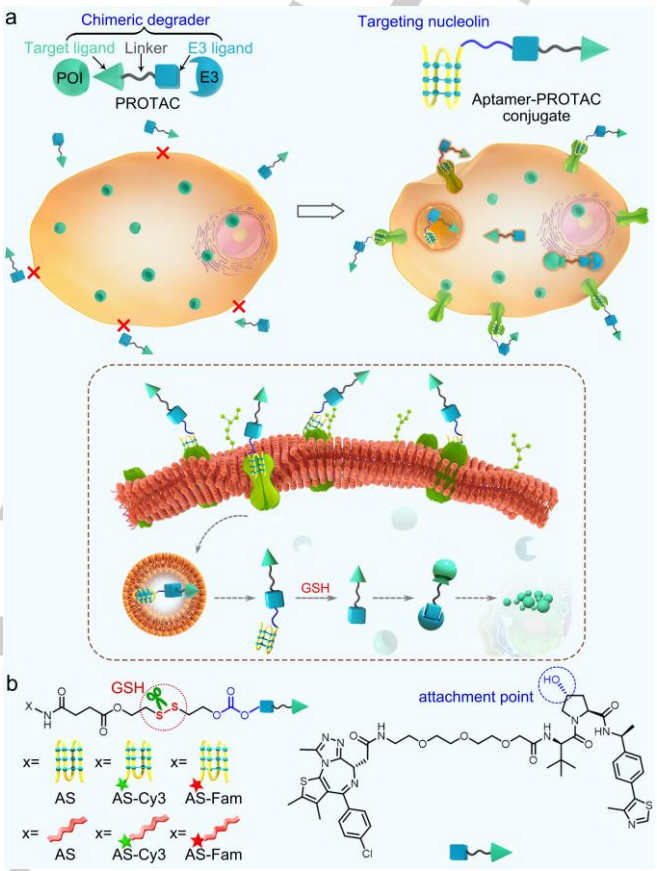

Figure 1. Design of AS-PROTAC conjugates. (**a**) Schematic diagram of the design strategy of APCs. The aptamer part of an APC selectively recognizes the cell membrane receptor and is specifically taken up into tumor cells. The cleavable linker is attacked by GSH to release the original PROTAC. (**b**) Chemical structures and design rationale of the APCs, imaging molecules and negative controls.

Synthesis of AS-PROTAC conjugates. The synthesis of APCs is outlined in Scheme 1. First, VHL ligand **1** (**Scheme S2** in **Supporting Information**) was condensed with dimethyl-4-oxo-3,8,11,14-tetraoxa-5-azahexadecan-16-oic acid to afford amide **2** in the presence of HATU and DIPEA. Then, the Boc protecting group was removed by TFA to give compound **3**, which was further condensed with intermediate **8** (**Scheme S1** in **Supporting Information**) in the presence of HATU and DIPEA to afford compound **4**. The hydroxyl group in compound **4** was reacted with 4-nitrophenyl chloroformate in the presence of DMAP to afford intermediate **5**. Key intermediate **7** was synthesized by reacting compound **5** with 2,2'-disulfanediylbis(ethan-1-ol) under catalysis by DMAP followed by esterification with succinic anhydride. Finally, compound **7** was conjugated with **AS** in the presence of Sulfo-NHS and EDCI to yield the APC **APR**. Next, the CRO-PROTAC conjugate (herein denoted compound **CPR**) and the Fam- or Cy3-modified

APR and APC conjugates (herein denoted compounds **APR**-Fam, **APR**-**Cy3**, **CPR**-**Fam** and **CPR**-**Cy3**) were synthesized using a protocol similar to that described for **APR** synthesis. ^{1}H-NMR and ^{13}C-NMR spectroscopy and high-resolution mass spectrometry (HRMS) were used to confirm the structures of key intermediates. The aptamer-modified conjugates were purified by reversed phase high-performance liquid chromatography (RP-HPLC) and confirmed by mass spectrometry (**Figures S7**-**S12** in **Supporting Information**).

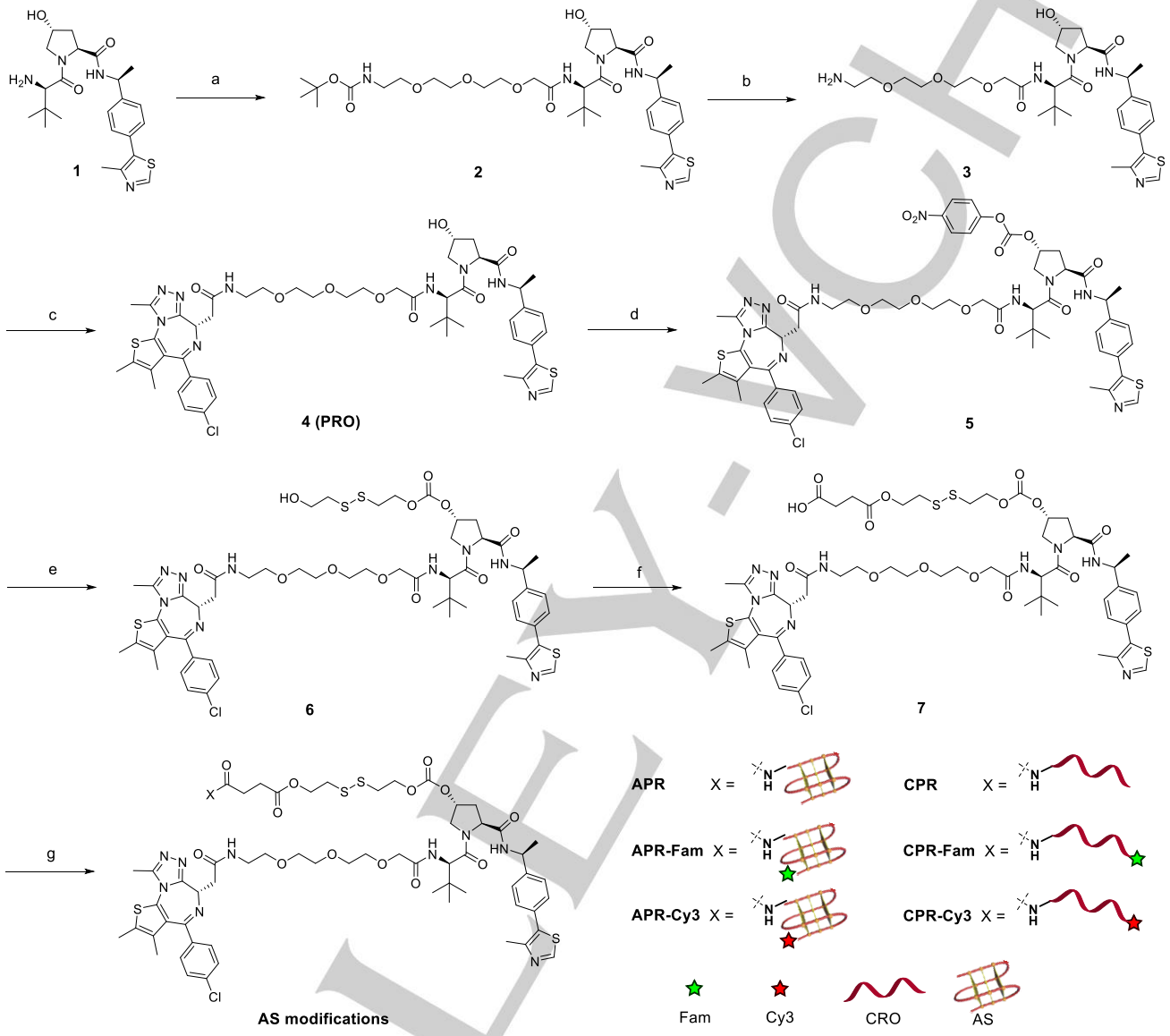

Scheme 1. Reagents and conditions: (**a**) Dimethyl-4-oxo-3,8,11,14-tetraoxa-5-azahexadecan-16-oic acid, HATU, DIPEA, DMF rt, 3 h, yield 75%. (**b**) CF_3COOH, DCM, rt, 6 h, yield 82%. (c) **8** (Scheme S1 in Supporting Information), **HA**TU, DIPEA, DMF, rt, 12 h, yield 70%. (**d**) 4-Nitrophenyl chloroformate, DMAP, DCM, rt, 12 h, yield 65%. (**e**) 2,2'-Disulfanediylbis(ethan-1-ol), DMAP, DCM, rt, 8 h, yield 68%. (**f**) Succinic anhydride, DMAP, DCM, rt, 3 h, yield 85%. (**g**) Aptamers, Sulfo-NHS, EDCI, dd-H_2O, DMF, 0.5 M Na_2CO_3/$NaHCO_3$, 12 h, yield 40-70%.

Stability of APR and release of PRO under reducing conditions. The stability of **APR** was evaluated by 10% polyacrylamide gel electrophoresis (PAGE). **AS**-**Cy3** and **APR**-**Cy3** were incubated in medium containing 10% fetal bovine serum (FBS) at 37 °C for different durations. **APR**-**Cy3**, like **AS**-**Cy3**, exhibited stable characteristics after incubation for 48 h in serum-containing medium. **APR**-**Cy3** almost existed as an intact form, implying that the terminal modification of **AS** with a PROTAC molecule did not reduce the degradation of **AS** (**Figure 2a**, **Figure S1** in **Supporting Information**). In addition, to further verify whether **PRO** can be effectively released from **APR**, an HPLC detection method was established to evaluate the in vitro release of **PRO** under reducing conditions (0.01 M dithiothreitol (DTT) in 1 × PBS buffer, pH = 7.4, 0.5% w/v Tween 80) at 37 °C (**Figure 2b**). The amount of free **PRO** released from **APR** was increased as the incubation time increased. Thus, the intensity of the detected **APR** peak was decreased, while the strength of the detected **PRO** and AS-CO-NH-R peaks was increased, implying the successful in vitro release of **PRO** from **APR** under the reducing conditions.

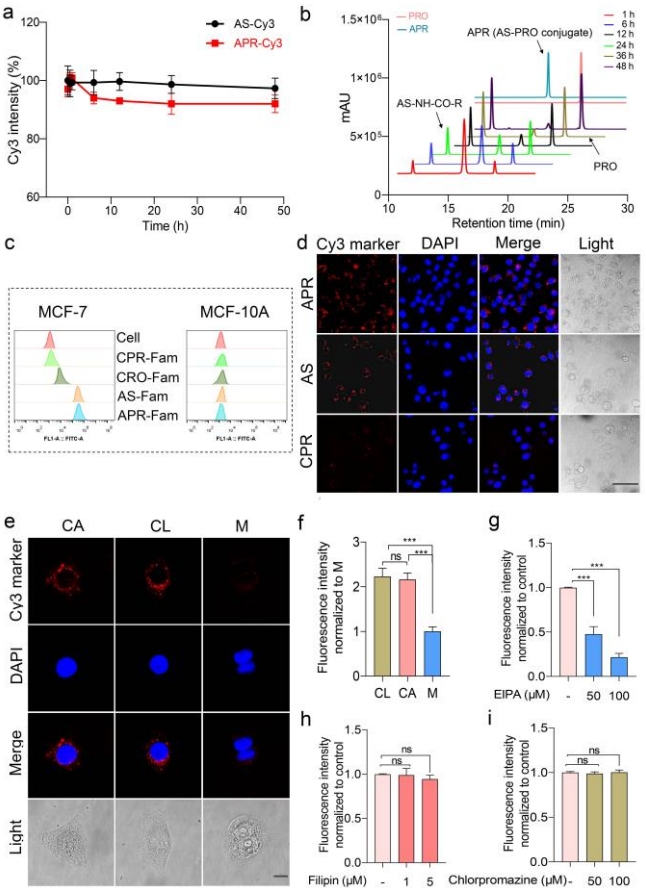

Figure 2. The stability and release for **APR** and the effects of AS-modified conjugates on cellular uptake and internalization. (**a**) Normalized concentrations of **AS**-**Cy3** and **APR**-**Cy3** in serum-containing medium over time. (**b**) HPLC chromatogram schematic diagram indicated drug-release profiles of **APR** in the reducing conditions and non-reducing conditions. (**c**) Flow cytometry results for MCF-7 cells and MCF-10A cells after incubation with 500 nM Fam-modified **AS**, **APR**, **CRO** and **CPR** for 0.5 h at 4°C. (**d**) Confocal laser scanning micrographs of target MCF-7 cells after treatment with 500 nM Cy3-modified **APR**, **AS** and **CPR** in DMEM at 37°C for 2 h. Scale bar, 20 μm. (**e**) Representative confocal micrographs of MCF-7 cells after pretreatment with inhibitors of endocytic pathways (CA, caveolae; CL, clathrin; M, macropinocytosis) and incubation with 500 nM Cy3-modified **APR**. Scale bar, 20 μm. (**f**-**i**) Chemical inhibition of cellular internalization of Cy3-modified **APR** in MCF-7 cells. Based on the control experiment (no inhibitor, **f**), the relative fluorescence of Cy3 was evaluated by flow cytometry after treatment with inhibitors of three endocytic pathways: EIPA (macropinocytosis, **g**), filipin (caveolae-mediated endocytosis pathway, **h**) or chlorpromazine (clathrin pathway, **i**). The error bars indicate the mean ± SD values; n = 3. $^{***}P < 0.005$; NS: no significant difference. The error bars indicate as the mean ± standard deviation (SD) values, n=3.

Effects of AS-modified conjugates on cellular uptake and internalization. To verify the uptake and internalization of **APR** by MCF-7 cells, flow cytometry and confocal laser scanning microscopy were carried out using Cy3- or Fam-modified conjugates. **AS** specifically targets cell membrane-localized nucleolin, which is overexpressed on MCF-7 breast cancer cells but not on MCF-10A (normal human mammary epithelial) cells.[18] Therefore, MCF-7 and MCF-10A cells were selected as nucleolin-positive and nucleolin-negative cells, respectively. First, flow cytometric analysis showed that both **AS**-**Fam** and **APR**-**Fam** exhibited much higher cellular uptake efficiency than the nonselective **CRO**-**Fam** and **CPR**-**Fam** conjugates after incubation with MCF-7 cells (**Figure 2c**). In contrast, after incubation with MCF-10A control cells, no differences between the fluorescence intensities of Fam-modified targeting and nontargeting oligonucleotides were observed. These results satisfactorily confirmed that **APR**-**Fam** can be specifically recognized by MCF-7 cells. Subsequently, we explored the uptake and specificity of **APR** through confocal laser scanning microscopy. MCF-7 cells were treated with **APR**-**Cy3**, **AS**-**Cy3** and **CPR**-**Cy3** for 1 h prior to staining with DAPI (Fam-modified samples were also examined). **Figure 2d** shows that cells incubated with **APR**-**Cy3** or **AS**-**Cy3** showed stronger red fluorescence than cells incubated with **CPR**-**Cy3**. Similar results were also observed after incubation with the Fam-modified conjugates (**Figure S2** in **Supporting Information**). These results suggested that the AS-conjugated PROTAC APR also maintained excellent and specific nucleolin-mediated internalization. In addition, when MCF-7 cells were pretreated with EIPA (an inhibitor of macropinocytosis), a dose-dependent decrease in the red fluorescence of **APR**-**Cy3** was detected (**Figure 2e**-**g**) compared with that in vehicle control-treated cells. However, an apparent Cy3 fluorescence signal was observed in the cytoplasm of MCF-7 cells pretreated with various concentrations of chlorpromazine (an inhibitor of the clathrin pathway) or filipin (an inhibitor of the caveolae-mediated endocytosis pathway) (**Figure 2h** and **2i**). This difference demonstrated that **APR**-**Cy3** was taken up by MCF-7 cells mainly through macropinocytosis. Interestingly, the mechanism of rapid internalization might provide a new strategy for improving the cell membrane permeability of PROTACs.

Effect of AS-modified conjugates on BET degradation. To further investigate the BET degradation activity and BET homolog selectivity of **APR**, Western blot analysis was performed by stimulating MCF-7 cells with different concentrations of **APR** and **CPR** (with **PRO** as the control) (**Figure 3a**-**d**). Both **APR** and **PRO** effectively degraded BRD4 in a concentration-dependent manner (**APR**: DC_{50} = 22 nM, D_{max} > 90%; **PRO**: DC_{50} = 13 nM, D_{max} > 90%), while almost no degradation of BRD4 was observed in **CPR**-treated cells. As shown in **Figure 3a** and **3b**, **APR** degraded only BRD4 and achieved excellent degradation efficiency at a concentration of 50 nM, whereas almost no degradation of BRD2 and BRD3 was observed at the same concentration. When the concentration was increased to 100 nM, the degradation rate of BRD2 and BRD3 mediated by **APR** was 65% and 58%, respectively. Slight degradation of BRD4 was observed in the **CPR** group when the **CPR** concentration was increased to 200 nM. These results verified that **APR** exhibited high efficiency for the degradation of BRD4 in nucleolin-overexpressing MCF-7 cells and that the **AS** modification had little effect on the degradation activity of the original **PRO**.

Effect of AS-modified conjugates on cytotoxicity. The antitumor activity of **APR** against MCF-7 and MCF-10A breast cancer cells was evaluated using a Cell Counting Kit-8 (CCK8) assay. In MCF-7 cells (**Figure 3e**, **Table S1** and **Figure S3** in **Supporting Information**), **APR** exhibited antiproliferative activity (IC_{50} = 56.9 nM) comparable to that of **PRO** (IC_{50} = 59.8 nM) and significantly superior to that of **CPR** (IC_{50} = 4.03 μM) and **AS** (IC_{50} = 2.60 μM). In contrast, the cytotoxicity of **APR** in MCF-10A cells was significantly decreased (IC_{50} = 3.13 μM) and was much lower than that of **PRO** (IC_{50} = 0.67 μM) and

comparable to that of **CPR** (IC_{50} = 3.54 μM) (**Figure 3f**). Moreover, the cytotoxicity of **AS** in MCF-10A cells within the tested concentration range was weak (IC_{50} = 6.90 μM). These results indicated that introduction of **AS** resulted in selective cytotoxicity of PROTACs in nucleolin-overexpressing MCF-7 cells. Notably, the observed selectivity may be due to the synergistic effect of the aptamer modification with the intrinsic properties of PRO. In addition, the effects of **APR** on MCF-7 cell apoptosis were evaluated (**Figure 3g**). After treatment with 100 nM **APR** and **PRO** for 48 h, the apoptosis rates of MCF-7 cells were 60.1% and 39.2%, respectively. However, the apoptosis rate of **CPR**-treated cells was decreased to 20.9% under the same conditions, which was significantly lower than that of **APR**-treated cells. The effects on apoptosis were consistent with the reductions in MCF-7 cell proliferation activity. Furthermore, a colony formation assay was performed to investigate the antiproliferative effects on MCF-7 cells (**Figure S4** in **Supporting Information**). Both **APR** and **PRO** effectively inhibited the growth of MCF-7 cell colonies in a concentration-dependent manner. Compared with unmodified **PRO**, **APR** exhibited improved selectivity toward the nucleolin-overexpressing MCF-7 cell line.

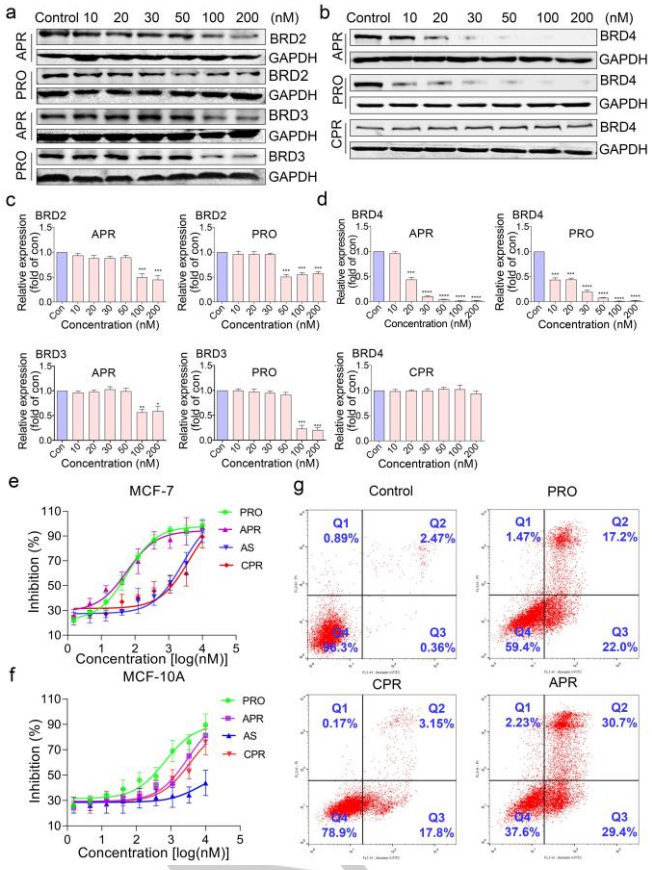

Figure 3. BET protein degradation and cytotoxicity of AS-modified conjugates. (**a**) Western blot analysis of the effects of compounds **APR** and **PRO** in inducing the degradation of BRD2 and BRD3 in MCF-7 cells after treatment for 24 h. (**b**) Effects of compounds **APR**, **PRO**, and **CPR** on the level of BRD4 in MCF-7 cells under the same conditions. GAPDH was used as the loading control. (**c**, **d**) Quantitative analysis of Western blot results using ImageQuant (Molecular Dynamics, US). The proteins BRD2, BRD3, and BRD4 were analyzed in MCF-7 cells. (**e**, **f**) Cytotoxicity of **APR**, **AS**, **CPR**, and **PRO** in target MCF-7 cells and nontarget MCF-10A cells, as determined by a CCK8 assay. (**g**) Apoptosis of target MCF-7 cells treated with different formulations.The data are presented as the mean ± SD values; n = 3. $^{*}P < 0.05$, $^{**}P < 0.01$, $^{***}P < 0.005$ and $^{****}P < 0.001$ vs the control group.

Effects of AS-modified conjugates on in vivo distribution. To test the tumor targeting profile of **APR**, imaging assays were used to investigate the tissue distribution of **APR**-**Cy3** in the MCF-7 xenograft mouse model, with **AS**-**Cy3** and **CPR**-**Cy3** as the controls. After administration via intravenous injection, the distribution of **AS**-**Cy3**, **APR**-**Cy3** and **CPR**-**Cy3** in tumors and major organs (heart, liver, spleen, lung and kidney) was analyzed (**Figure 4a**). The fluorescence intensity of Cy3 in tumor tissues of **APR**-**Cy3**-treated mice was significantly higher than that in **AS**-**Cy3**-treated mice 4 h after administration. However, almost no Cy3 fluorescence was observed in the tumor tissues of **CPR**-treated mice. In addition, all three compounds were distributed mainly in the liver and kidneys. Eight hours after administration, the fluorescence intensity of Cy3 in the tumor tissues of **APR**-**Cy3**-treated mice was still higher than that in **AS**-**Cy3**-treated mice, while there was no Cy3 fluorescence was observed in the tumor tissues of **CPR**-**Cy3**-treated mice. Furthermore, no fluorescence signal was detected in the heart, spleen or lung in mice in any of the three groups at either of the two time points. To further verify whether the **AS**-**PRO** conjugate exhibited tumor targeting ability in MCF-7 xenografts, we additively tested the distribution of **APR**-**Cy3** in mice and evaluated its aggregation in vivo (**Figure 4b**). Similar to the previous experiments, **AS**-**Cy3** and **CPR**-**Cy3** were selected as the controls. Interestingly, **APR**-**Cy3** was able to recognize MCF-7 tumor cells and aggregate in the tumors because the fluorescence retention time of **APR**-**Cy3** fluorescence in tumor tissues was much longer than that of **CPR**-**Cy3** and **AS**-**Cy3** in the control groups. Moreover, strong fluorescence signals were still observed in tumors 8 h after the injection, whereas no fluorescence signal was observed in the tumors of **CPR**-**Cy3**-treated mice. These results indicated that **APR** exhibited excellent tumor targeting ability in the MCF-7 xenograft model.

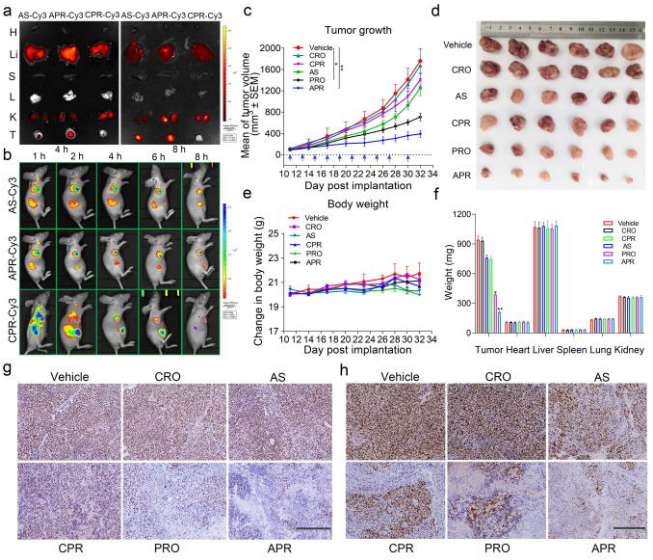

Figure 4. The distribution and in vivo antitumor efficacy of **AS**-modified conjugates in mice bearing MCF-7 xenografts. (**a**, **b**) In vivo distribution of **AS**-**Cy3**, **APR**-**Cy3**, and **CPR**-**Cy3** in major organs (H, heart; Li, liver; S, spleen; L, lung; and K, kidney) and the tumor (T) after intravenous injection. (**c**) Changes

in the tumor volume during the 21-day period of treatment via intravenous injection at a dosing frequency of every other day. The blue arrows indicate the dosing time points. (**d**) Macroscopic views of xenograft tumors in the different groups after 21 days of the indicated treatments. (**e**) Changes in the body weight of xenografted mice during the 21-day period of treatment with the different formulations indicated. The blue arrows indicate the dosing time points. (**f**) Analysis of tumor and organ weights during the 21-day period of treatment with the different formulations indicated via intravenous injection at a dosing frequency of every other day. Immunohistochemistry of tumor tissues in the different treatment groups. (**g**) Micrographs of tumor tissue sections with Ki67 staining from the six treatment groups. (**h**) Micrographs of tumor tissue sections with BRD4 staining from the six treatment groups. Scale bar, 200 μm.

Effect of AS-modified conjugates on in vivo efficacy and toxicity. Given the encouraging antitumor activity and targeted distribution profiles, the in vivo antitumor efficacy of **APR** was evaluated in the MCF-7 xenograft mouse model. When the tumors had an average volume of 150 mm^3 after implantation, mice were randomly divided into six groups. PBS or **AS**, **CRO**, **PRO**, **CPR** or **APR** at a DNA dose of 10 μM (equal to a dose of 10 mg/kg for **PRO**) was administered intravenously every other day. As shown in **Figure 4c** and **4d**, **PRO** effectively inhibited tumor growth and achieved a good tumor growth inhibition (TGI) rate of 59.8% after 21 days of treatment. In contrast, **CRO** did not exhibit antitumor activity in vivo. Interestingly, **APR** showed excellent in vivo antitumor efficacy, with a TGI rate of 77.5%, indicating that **APR** was significantly more potent than **CPR** (TGI = 20.2%) and **AS** (TGI = 28.8%) (**Figure S5** in **Supporting Information**). In addition, the toxicity of **APR** in the xenograft mouse model was further evaluated. The body weight of treated mice was measured every 3 days during the treatment period (**Figure 4e**). All compounds were well tolerated in the treated groups, without significant body weight loss and obvious adverse effects. Next, the main organs of the treated mice were weighed to evaluate toxicity (**Figure 4f**). There were no significant differences in the weights of individual organs among the different groups. Furthermore, H&E staining was used to evaluate the toxicity of **AS** modifications (**Figure S6** in **Supporting Information**). Analysis of the H&E-stained sections of major organs revealed severe lung lesions in xenografted mice treated with **PRO** and **CPR**. In contrast, no significant damage to any major organ was observed in **APR**-treated mice. These results were consistent with those of previous studies showing that **AS** modification is helpful for decreasing the severity of lung lesions.[18a] Immunohistochemistry was employed to investigate the TGI efficacy of **APR**. **APR** performed better in inducing apoptosis than either control compound (**Figure 4g**). The number of Ki67-stained cells in the **APR** group was significantly lower than that in the other groups, implying that **APR** had the best TGI efficacy. To further explore the in vivo BRD4 degradation efficiency, immunohistochemistry was performed using an anti-BRD4 antibody. As shown in **Figure 4h**, compared with the blank control, compounds **CRO** and **AS** led to only slight changes in BRD4 expression, while BRD4 expression was significantly decreased in the **PRO**- and **APR**-treated groups. Notably, **APR** more effectively decreased the expression of BRD4 than **PRO**, suggesting that **AS** modification enhanced BRD4 degradation in mice.

Conclusion

In summary, a novel strategy for modifying PROTACs with an aptamer was developed to overcome the limitations of conventional PROTACs. We demonstrated for the first time that aptamer conjugation facilitates the improvement of tumor targeting specificity, leading to enhanced in vivo antitumor activity and protein degradation and reduced toxicity. Thus, the innovative APC technology established in this work has the potential to improve the drug-likeness of conventional PROTACs. Importantly, this aptamer modification strategy may have broad applications in targeted protein degradation due to the advantages of aptamers in precision medicine. Our future efforts will be aimed at exploring diverse aptamers and designing new types of linkers for better tumor tissue specificity and clinical efficacy.

Acknowledgements

This work was supported by the National Natural Science Foundation of China (grant 82030105 to C. S., 82003567 to S. H., and 81725020 to C. S), the National Key Research and Development Program of China (grant 2020YFA0509100 to C. S.) and National Natural Science Foundation of Shanghai (grant 21ZR1422600 to F. G.).

Keywords: Aptamers • BET • Drug design • PROTAC • Tumor-specific Targeting

[1] a) Y. Zou, D. Ma, Y. Wang, *Cell Biochem. Funct.* **2019**, *37*, 21-30; b) M. Pettersson, C. M. Crews, *Drug Discov Today Technol* 2019, *31*, 15-27.
[2] P. Ottis, C. M. Crews, *ACS Chem. Biol.***2017**, *12*, 892-898.
[3] A. C. Lai, C. M. Crews, *Nat. Rev. Drug Discovery* **2017**, *16*, 101-114.
[4] C. A. Lipinski, *Drug Discov Today: Technol.* **2004**, *1*, 337-341.
[5] a) S. Gu, D. Cui, X. Chen, X. Xiong, Y. Zhao, *Bioessays* **2018**, *40*, 1700247; b) S. D. Edmondson, B. Yang, C. Fallan, *Bioorg. Med. Chem. Lett.* **2019**, *29*, 1555-1564; c) K. Raina, C. M. Crews, *Curr. Opin. Chem. Biol.***2017**, *39*, 46-53.
[6] Y. Wang, X. Jiang, F. Feng, W. Liu, H. Sun, *Acta Pharm. Sin. B* **2020**, *10*, 207-238.
[7] a) M. Yuan, L.-L. Huang, J.-H. Chen, J. Wu, Q. Xu, *Signal Transduction Targeted Ther.* **2019**, *4*:16; b) P. R. Halliday, C. M. Blakely, T. G. Bivona, *Curr. Oncol. Rep.* **2019**, *21*,21; c) D. C. Mastellos, D. Ricklin, J. D. Lambris, *Nat. Rev. Drug Discovery* **2019**, *18*, 707-729.
[8] a) P. S. Dragovich, T. H. Pillow, R. A. Blake, J. D. Sadowsky, E. Adaligil, P. Adhikari, S. Bhakta, N. Blaquiere, J. Chen, J. Dela Cruz-Chuh, K. E. Gascoigne, S. J. Hartman, M. He, S. Kaufman, T. Kleinheinz, K. R. Kozak, L. Liu, L. Liu, Q. Liu, Y. Lu, F. Meng, M. M. Mulvihill, A. O'Donohue, R. K. Rowntree, L. R. Staben, S. T. Staben, J. Wai, J. Wang, B. Wei, C. Wilson, J. Xin, Z. Xu, H. Yao, D. Zhang, H. Zhang, H. Zhou, X. Zhu, *J. Med. Chem.* **2021**, *64*, 2534-2575; b) P. S. Dragovich, T. H. Pillow, R. A. Blake, J. D. Sadowsky, E. Adaligil, P. Adhikari, J. Chen, N. Corr, J. Dela Cruz-Chuh, G. Del Rosario, A. Fullerton, S. J. Hartman, F. Jiang, S. Kaufman, T. Kleinheinz, K. R. Kozak, L. Liu, Y. Lu, M. M. Mulvihill, J. M. Murray, A. O'Donohue, R. K. Rowntree, W. S. Sawyer, L. R. Staben, J. Wai, J. Wang, B. Wei, W. Wei, Z. Xu, H. Yao, S. F. Yu, D. Zhang, H. Zhang, S. Zhang, Y. Zhao, H. Zhou, X. Zhu, *J. Med. Chem.* **2021**, *64*, 2576-2607; c) M. A. Maneiro, N. Forte, M. M. Shchepinova, C. S. Kounde, V. Chudasama, J. R. Baker, E. W. Tate, *ACS Chem. Biol.* **2020**, *15*, 1306-1312.
[9] J. Liu, H. Chen, Y. Liu, Y. Shen, F. Meng, H. U. Kaniskan, J. Jin, W. Wei, *J. Am. Chem. Soc.* **2021**, doi. org/10.1021/jacs.1c00451.
[10] Z. Li, B.-F. Krippendorff, D. K. Shah, *Pharm. Res.* **2017**, *34*, 2131-2141.
[11] A. Beck, L. Goetsch, C. Dumontet, N. Corvaia, *Nat. Rev. Drug Discovery* **2017**, *16*, 315-337.
[12] A. Wagh, H. Song, M. Zeng, L. Tao, T. K. Das, *Mabs* **2018**, *10*, 222-243.

[13] a) C. Tuerk, L. Gold, *Science (New York, N.Y.)* **1990**, *249*, 505-510; b) D. H. J. Bunka, P. G. Stockley, *Nat. Rev. Microbiol.* **2006**, *4*, 588-596.

[14] P. Kalra, A. Dhiman, W. C. Cho, J. G. Bruno, T. K. Sharma, *Front. Mol. Biosci.* **2018**, *5:* 14.

[15] J. Zhou, J. Rossi, *Nat. Rev. Drug Discovery.* **2017**, *16*, 181-202.

[16] K. W. Thiel, P. H. Giangrande, *Ther. Delivery.* **2010**, *1*, 849-861.

[17] S. Soundararajan, L. Wang, V. Sridharan, W. Chen, N. Courtenay-Luck, D. Jones, E. K. Spicer, D. J. Fernandes, *Mol. Pharmacol.* **2009**, *76*, 984-991.

[18] a) F. Li, J. Lu, J. Liu, C. Liang, M. Wang, L. Wang, D. Li, H. Yao, Q. Zhang, J. Wen, Z. K. Zhang, J. Li, Q. Lv, X. He, B. Guo, D. Guan, Y. Yu, L. Dang, X. Wu, Y. Li, G. Chen, F. Jiang, S. Sun, B. T. Zhang, A. Lu, G. Zhang, *Nat. Commun.* **2017**, *8*, 1390; b) J. He, T. Peng, Y. Peng, L. Ai, Z. Deng, X. Q. Wang, W. Tan, *J. Am. Chem. Soc.* **2020**, *142*, 2699-2703.

[19] a) J. E. Rosenberg, R. M. Bambury, E. M. Van Allen, H. A. Drabkin, P. N. Lara, Jr., A. L. Harzstark, N. Wagle, R. A. Figlin, G. W. Smith, L. A. Garraway, T. Choueiri, F. Erlandsson, D. A. Laber, *Invest. New Drugs* **2014**, *32*, 178-187; b) R. Yazdian-Robati, P. Bayat, F. Oroojalian, M. Zargari, M. Ramezani, S. M. Taghdisi, K. Abnous, *Int. J. Biol. Macromol* **2020**, *155*, 1420-1431.

[20] N. Wang, R. Wu, D. Tang, R. Kang, *Signal Transduction Targeted Ther.* **2021**, *6*, 23.

[21] C. Y. Yang, C. Qin, L. Bai, S. Wang, *Drug Discovery Today: Technol.* **2019**, *31*, 43-51.

[22] a) M. S. Gadd, A. Testa, X. Lucas, K. H. Chan, W. Chen, D. J. Lamont, M. Zengerle, A. Ciulli, *Nat. Chem. Biol.* **2017**, *13*, 514-521; b) P. Pfaff, K. T. G. Samarasinghe, C. M. Crews, E. M. Carreira, *ACS Cent. Sci.* **2019**, *5*, 1682-1690.

[23] F. J. Cimas, E. Niza, A. Juan, M. D. M. Noblejas-Lopez, I. Bravo, A. Lara-Sanchez, C. Alonso-Moreno, A. Ocana, *Pharmaceutics* **2020**, *12*. 986

[24] J. H. Min, H. Yang, M. Ivan, F. Gertler, W. G. Kaelin, Jr., N. P. Pavletich, *Science* **2002**, *296*, 1886-1889.

[25] a) Q. S. Pan, C. P. Nie, Y. L. Hu, J. T. Yi, C. Liu, J. Zhang, M. M. He, M. Y. He, T. T. Chen, X. Chu, *ACS Appl. Mater. Interfaces* **2020**, *12*, 400-409; b) M. Ye, X. Wang, J. Tang, Z. Guo, Y. Shen, H. Tian, W. H. Zhu, *Chem. Sci.* **2016**, *7*, 4958-4965.

…

10.1002/anie.202107347

Entry for the Table of Contents

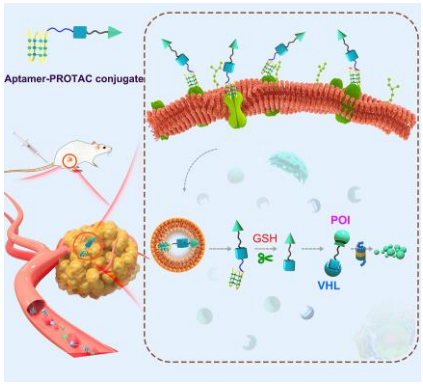

The first aptamer-PROTAC conjugate (APC) was designed to improve the tumor specific targeting and in vivo antitumor potency of conventional PROTACs. This strategy may pave the way for the design of tumor-specific targeting PROTACs and have broad applications in PROTAC-based drug development.